Bioresource Technology 320 (2021) 124251

Contents lists available at ScienceDirect

Bioresource Technology

journal homepage: www.elsevier.com/locate/biortech

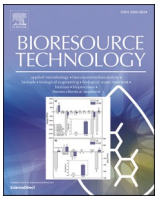

Effects of surface skewness on local shear stresses, biofilm activity, and microbial communities for wastewater treatment

Philip M. Roveto [a,1], Adwaith Gupta [b], Andrew J. Schuler [a,*]

[a] University of New Mexico, 1 University Blvd, Albuquerque, NM 87131, United States
[b] Paanduv Applications, 124 Parwana Nagar, Bareilly, UP 243122, India

HIGHLIGHTS

- Negative skewness led to most rapid biofilm growth and nitrate production.
- Computational fluid dynamics modeling provided insights to local shear conditions.
- Microbial populations on skewed surfaces diverged from those on flat surfaces.
- Skewness most important when biomass had not overgrown surface features.

ARTICLE INFO

Keywords:
Biofilms
Attachment
Roughness
Skewness
Nitrification
Computational fluid dynamics
16s rRNA amplicon sequencing

ABSTRACT

This study's objective was to assess attachment surface skewness (asymmetric surface height variation) effects on biofilm development. 3D printed molds were used to create surfaces with 300 μm features to provide opposite skewness but identical roughness values. Surfaces with negative skewness had consistently greater nitrite oxidation and biomass growth than other surfaces during biofilm development when studied in annular bioreactor systems. CFD modelling predicted local shear stress differences that could explain experimental results. 16 s rRNA gene amplicon sequencing revealed population differences, including relatively high *Acinetobacter* and *Terrimonas* fractions on the negative skew surfaces, and PCoA analyses indicated the flat surface populations diverged from the skew surfaces by the study's end. The results suggest skewness is particularly important in systems where biofilms have not overgrown surface features, as in system startup, thin biofilms, and shorter time frame studies, which includes much previous microbial attachment research.

1. Introduction

It is well recognized that biofilms are of great importance to human health and welfare, including their potential negative effects on public health (such as increased pathogen resistance to antibiotics) and economics (such as pipeline corrosion and increased friction) (Crawford et al., 2012; Hall-Stoodley et al., 2004; Whitehead and Verran, 2006). Biofilms are also highly beneficial in many engineered systems, such as bioreactors for industrial processes and wastewater treatment. The effects of surface properties on microbial adhesion and biofilm development are therefore of great interest in a variety of environments, and the goals of surface selection/design can be to reduce or enhance biofilm growth and microbial activity.

Much previous research has demonstrated that surface roughness (typically defined as the root mean square deviation of surface height) greatly affects bacterial attachment, but roughness measurements do not provide an indication of the distribution and shape of surface features (Crawford et al., 2012). While roughness has generally been found the positively correlate with adhesion, this is not always true; for example, the addition of well-defined surface features at the micron scale has been found to reduce the biofilm adhesion of a pure culture (Chung et al., 2007). Skewness, defined as the third moment of the density function, is a measure of the asymmetric distribution of surface height (Tayebi and Polycarpou, 2004). Positive skewness values indicate surfaces with sharper peaks and more rounded valleys, while negative skewness values indicate surfaces more rounded peaks with sharper valleys (see

* Corresponding author.
E-mail addresses: pmroveto@garverusa.com (P.M. Roveto), adwaith@paanduv.com (A. Gupta), schuler@unm.edu (A.J. Schuler).
[1] Present address: Garver, 2049 E Joyce Blvd, Fayetteville, AR 72703, United States.

https://doi.org/10.1016/j.biortech.2020.124251
Received 13 August 2020; Received in revised form 5 October 2020; Accepted 8 October 2020
Available online 23 October 2020

examples in the Materials and Methods section below). Skewness has been shown to be important to tribological surface properties, with more negative skewness associated with reduced sliding friction (Sedlacek et al., 2012).

Little is known about skewness effects on bacterial adhesion, and so they have been recommended for further study (Crawford et al., 2012). This knowledge exists in part because other parameters, such as roughness, tend to vary in biofilm and bacterial adhesion studies where skewness has been reported, and so there is therefore a lack of studies where such variables are controlled. Nevertheless, previous research provides clues that skewness may be important to adhesion and growth. For example, Singh et al. (2011) found that lower skewness values corresponded with higher rates of cellular attachment, including for *Staphylococcus aureus*, but because roughness and feature size co-varied with skewness the role of skewness alone could not be determined. Similarly, Lüdecke et al. (2014) reported much higher rates of *Escherichia coli* attachment to a material with negative skewness than on 3 materials with positive skewness, however other parameters such as roughness, hydrophobicity, and surface feature height varied greatly between the surfaces. The skewness of activated-carbon-coated microbial fuel cell cathode surfaces was positively correlated with performance reported by Santoro et al. (2014), but again other surface parameters varied in their study.

Nitrifying biofilms are diverse microbial communities that feature chemoautotrophic ammonia-oxidizing bacteria (AOB) that oxidize ammonia to nitrite (NO_2^-), nitrite-oxidizing bacteria (NOB) that oxidize nitrite to nitrate (Balows et al., 1992), and also contain heterotrophic bacteria (Ren et al., 2014). Biofilms can provide long residence times in bioreactors, and so they are often used to enrich for slow growing autotrophic nitrifiers in wastewater treatment systems (Martens-Habbena et al., 2009; Nowka et al., 2015) such as trickling filters (van den Akker et al., 2011), integrated fixed film activated sludge, and moving bed biofilm reactors (MBBRs, Song et al., 2019). Previous work has suggested rates of nitrogen removal from wastewater can be increased through the design of biofilm attachment surface chemical characteristics (Khan et al., 2011, 2013; Kim et al., 1997; Klaus et al., 2016; Roveto and Schuler, 2019).

There is currently a knowledge gap in the literature with respect to skewness effects on mixed microbial community biofilm formation, including those used for nitrification in wastewater treatment, nor are there previous studies of bacterial adhesion with surface skewness as a well-defined independent variable. It was hypothesized that surface skew can affect biofilm structure (including population composition), and function, in part because local shear forces (at scales less than surface features) and velocity gradients are likely to differ across surfaces with different skewness characteristics, which should in turn affect attachment and mass transfer of substrates and wastes in and out of the biofilms. For example, a negative skew surface may have smaller protected areas (valleys) with relatively low velocity gradients, while a positive skew surface is expected to have larger valleys containing such relatively low velocity gradients.

The objective of this research was to determine whether surface skewness can affect biofilm formation, performance, and microbial community composition under well-defined conditions, using nitrification in wastewater as a model system. This work maybe useful to determine whether surface skewness can be a useful design parameter, and more generally to understand whether the non-engineered skewness inherent to any surface can affect biofilm formation and function. The experimental approach was to grow biofilms in annular bioreactors (to provide well-defined mixing) on 3 engineered silicone surfaces with well-defined skewness values: a flat surface, a surface with positive skew, and a surface with negative skew. Experimental replicates were included to assess reproducibility (6 reactors total). Biofilm growth, nitrifying activity, 16 s rRNA gene amplicon sequencing, and computational fluid dynamics (CFD) modeling were employed to better understand how skewness affected biofilm formation and longer term structure and function.

2. Materials and methods

2.1. Experimental systems

Three elastomeric silicone surfaces were constructed with well-defined features using a combination of 3D printing and silicone molding. First, a 24 × 16 × 0.4 cm a negatively skew surface mold was created by 3D printing (Replicator 2, Makerbot Industries LLC, Brooklyn, NY). The 3D printed surface consisted of 300 μm wide semi-cylindrical rows formed by the 3D printing process as acrylonitrile butadiene styrene (ABS) filament was extruded through a 300 μm nozzle. This 3D printed surface was used as mold to produce a mirror image (positive skew) surface by pouring uncured silicone (1:1 Elastomer Kit, Smooth-On, Macungie, PA) into it. After curing overnight, the silicone film was peeled out of the mold, yielding the positive skewness surface (Fig. 1a). The negative skew surface (Fig. 1b) was synthesized similarly, except the mold was a positive skew silicone surface formed as described in the previous step. The flat surface was constructed by pouring uncured silicone into a flat tray to a depth of 2 mm. The skewed surfaces had identical calculated root mean square roughness (R_q; 33 μm), arithmetic mean roughness (R_a; 27 μm), and kurtosis (κ; 0.50) values, but they had opposite skewness values (γ; ±1.15).

Annular bioreactors, consisting of cylindrical outer vessels and inner rotating cores, have been frequently used for biofilm studies because they provide facile control of reasonably well-defined cross-flow velocities. A novel, low cost set of annular bioreactors was constructed using a 6-paddle gang stirrer (Phipps & Bird, Richmond, VA) modified to carry six 3D printed inner cylinders (height 3 cm, radius 6.4 cm; Fig. 1c). The 6 silicone films (experimental replicates with positive skewness, negative skewness, and flat surfaces) were attached to the curved surface of the inner cylinders with silicone sealant, resulting in cylinders (height 40 cm, radius: 6.6 cm) with skewed feature rows oriented perpendicular to the direction of rotation, which were fastened to the 6 axles of the gang stirrer. The total area of the attachment surfaces was 166 cm^2 per bioreactor. The inner cylinders were then placed in 7.0 cm inner radius acrylic cylinder reactors, providing an interstitial gap of 0.4 cm. This process yielded a 6 reactor series with a single controller to provide uniform rotation (Fig. 1c). The bioreactors were fitted with submerged inlets below the inner cylinders and overflow outlets for continuous flow. Peristaltic pumps provided nutrient feed at a rate of 3.0 L/d (2.06 mL/min) and the working volume was 1.5 L, yielding a hydraulic retention time of 12 h. The reactors were not aerated but were open to the atmosphere, and oxygen concentrations were greater than 4 mg/L throughout the experiment.

The biofilm surfaces were inoculated by submersion in a 1:1 mixture of activated sludge and primary effluent from the Albuquerque Southside Water Reclamation Facility (SWRF) for 2 h while rotating at 120 RPM. The SWRF includes an A_2O-type activated sludge configuration performing nitrification and denitrification. After inoculation, all bioreactor surfaces were wiped clean except the outer silicone attachment surfaces, the inoculation mixture was replaced with synthetic feed, and rotation at 120 RPM was resumed. The synthetic feed was as described previously (Roveto and Schuler, 2019) and contained the following: NH_4Cl, 25 mg-N/L; $NaNO_2$, 5.5 mg-N/L; Na_2HPO_4-H_2O, 5.0 mg-P/L; $CaCl_2$-$2H_2O$, 8.0 mg-Ca/L; $MgSO_4$-$7H_2O$, 2.0 mg-Mg/L; KCl, 2.6 mg-K/L; Na_2EDTA-$2H_2O$, 7.0 mg/L; $FeSO_4$-$7H_2O$, 2.0 mg-Fe/L; $ZnSO_4$-$7H_2O$, 0.98 mg-Zn/L; $MnSO_4$-H_2O, 0.275 mg-Mn/L; $CuSO_4$-$5H_2O$, 0.064 mg-Cu/L; Na_2MoO_4-$2H_2O$, 0.014 mg-Mo/L. The pH was 6.8 – 7.2, with 200 mg/L $NaHCO_3$ included as buffer.

2.2. Analytical measurements

2.2.1. Nitrogen

Samples were taken near the effluent ports, filtered (0.45 μm syringe

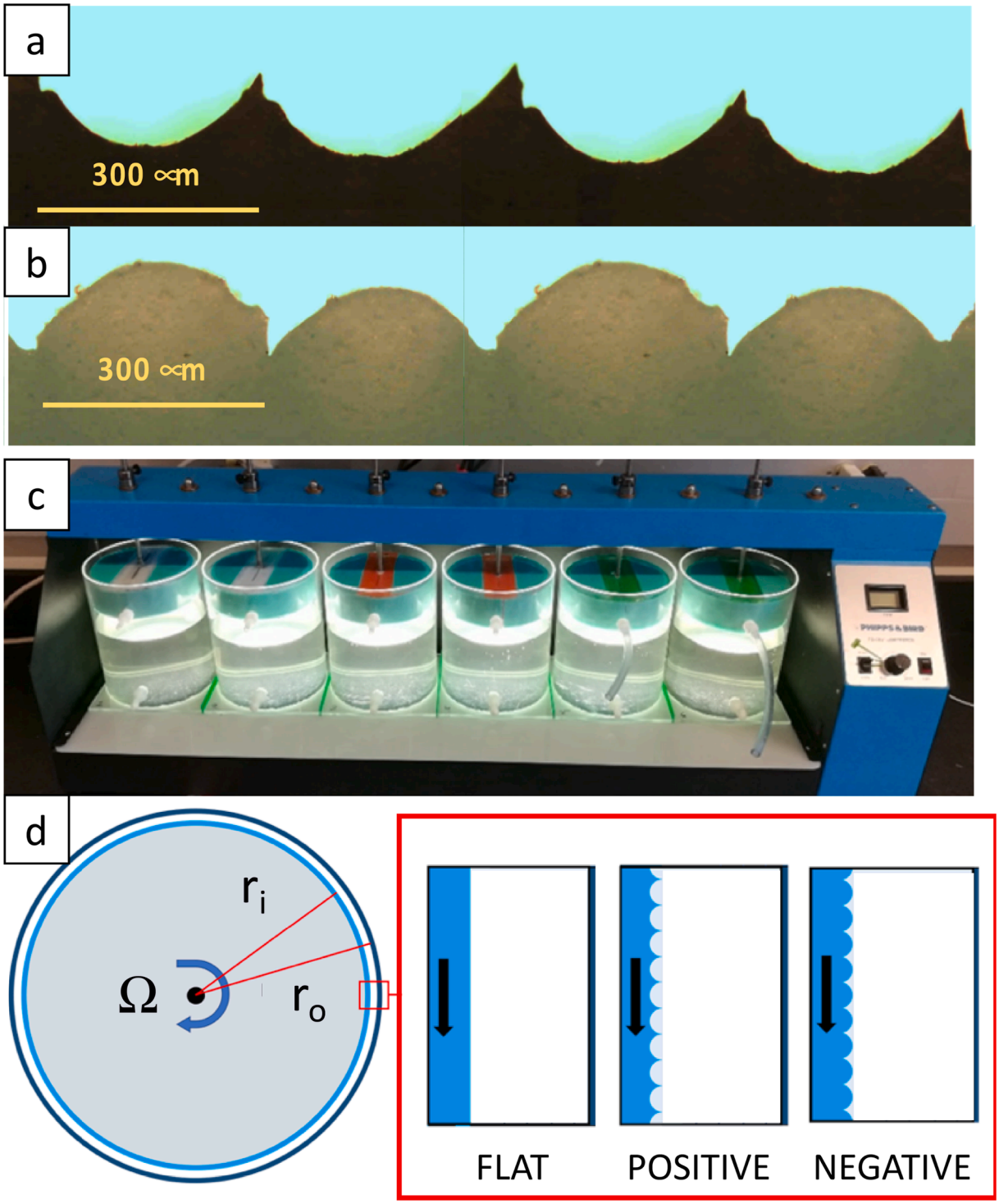

Fig. 1. Experimental system. Silicone surfaces with (a) positive and (b) negative skewness values, respectively, imaged using light microscopy (scale bar: 300 μm). (c) silicone surfaces in annular bioreactors (shown just before rotating surfaces were submerged in liquid media) with modified gang stirrer. Influent and effluent ports, but not tubing, are shown. (d) Plan view schematic of annular bioreactor with inner cylinder (radius r_i) rotating with annular speed (Ω) inside of stationary cylinder (radius r_o), with 3 different surfaces attached to inner cylinder shown in detail to right.

type; Millipore-Sigma, USA), and they were immediately analyzed or frozen at −4 °C. Ammonia concentrations were determined colorimetrically using the salicylate method (Method 10031; Hach, Loveland, CO, USA). Nitrite and nitrate were measured by ion chromatography (ICS-3000, Dionex, Sunnyvale, CA, USA) using an anion-specific analytical column (ThermoScientific, Waltham, MA, USA). Concentrations of frozen effluent samples were checked for consistency by comparing samples immediately after filtration with those that had been filtered and tested after 6 days of storage at −4 °C with no measurable differences observed. Fluxes (g-N/m^2/d) were calculated by multiplying the removal or accumulation rates by the reactor liquid volume and dividing by the biofilm attachment surface area. Nitrogen mass balances were calculated based on total nitrogen species measured for reactor influent and effluent to confirm analytical results. Nitrogen measurements were

taken from each bioreactor yielding datasets from experimental duplicates of each surface topography (flat, positive skew, and negative skew). Statistical testing for significant differences between the surfaces was determined based on 6 to 10 measurements of each surface unless otherwise noted, as described in Section 2.4.

2.2.2. Biomass

Suspended biomass was determined using Standard Method 10030, (American Public Health Association et al., 2005). Attached biomass was determined by removing a sacrificial piece of silicone from each of the 6 surfaces (5–10 cm^2 on day 26, 134 cm^2 on day 56, the experiment end), drying for 1 h at 105 °C and weighing. Replacement material was attached using silicone sealant on day 26. The surfaces were then cleaned with 0.2% sulfuric acid, rinsed with DI, dried at 105 °C and weighed, and the attached biomass mass was determined by subtraction. Weight loss by bare silicone controls was negligible.

Scanning electron microscopy (SEM) was performed as follows: samples of biofilm-attached silicone surfaces were cut from the cylindrical carriers and immediately fixed by rinsing with 1X PBS, submerging in 2.5% glutaraldehyde (Sigma Aldrich, St. Louis, MO) for 3 h, rinsing with PBS, submerging in 0.1% OsO_4 (Electron Microscopy Sciences, Hatfield, PA) for 30 min, rinsing with PBS, and dehydrating with an ethanol progression of 30%, 50%, 70%, 90%, 100% for 10 min each. Samples were dried under vacuum at room temperature for 24 h. Fixed biofilm samples were coated with an Au-Pd alloy through evaporative sputtering with a thickness of 200 Ã…. Observations were performed with a JEOL 5800LV scanning electron microscope, using an accelerating current of 10 kV and a probe current of 30nA. Representative images of biomass coverage were chosen from 20 images of each topographical surface.

2.2.3. Microbial communities

16 s rRNA amplicon sequencing was performed using the Illumina MiSeq platform (Illumina, Inc., San Diego, CA, USA). All analyses were done on each of 2 experimental replicates and average values were reported. DNA extraction, amplification, and sequencing were performed by MRDNA (Shallowater, TX, USA). DNA extraction was performed using a PowerSoil DNA Extraction kit by the manufacturer's instructions (Qiagen, Germantown, MD, USA). Polymerase chain reaction (PCR) amplification was done using the universal prokaryote primers 515F and 806R, which target the V4 region of the 16 s rRNA gene (Turner et al., 1999), including barcodes placed on the forward primer. A 30-cycle reaction was used (5 cycles for PCR products) with the HotStarTaq Plus Master Mix Kit (Qiagen) under the following conditions: 94 °C for 3 min, and 28 cycles of 94 °C for 30 s, 53 °C for 40 s and 72 °C for 1 min, followed by 72 °C for 5 min for final elongation. PCR products were checked in 2% agarose gel to determine the success of amplification. Multiple amplicon samples were pooled together in equal proportions based on their molecular weight and DNA concentrations. Pooled samples were purified using calibrated Ampure XP beads. The pooled and purified PCR products were used to prepare the DNA sequence library following the Illumina MiSeq protocol. Briefly, sequences were joined, depleted of barcodes, sequences < 150 bp were removed, and sequences with ambiguous base calls were removed. Sequences were denoised, operational taxonomic units (OTUs) were generated, and chimeras were removed. OTUs were defined by clustering at 97% similarity. Final OTUs were taxonomically classified using BLASTn against a curated database derived from GreenGenes, RDPII and NCBI (DeSantis et al., 2006).

2.3. Hydrodynamic calculations

Reynolds numbers were calculated considering flow between 2 coaxial cylinders (Taylor-Couette flow) using Eq. (1), where Ω was the angular velocity of the inner cylinder (rad/s), d was the distance between the inner and outer cylinders (m), r_o was the radius of the outer cylinder, and ν was the kinematic viscosity of water (m^2/s) (Andereck et al., 1986). For comparison with CFD model predictions, shear stress (τ) was calculated for a simplified system with consisting of two parallel, flat, sliding plates (planar Couette flow) using Eq. (2), where μ = dynamic viscosity (Pa·s).

$$Re = \frac{\Omega r_o d}{\nu} \quad (1)$$

$$\tau = \mu \frac{\Omega r_o}{d} \quad (2)$$

CFD modeling was performed using the open source software OpenFOAM (Weller et al., 1998) by Paanduv Applications (www.paanduv.com) to provide insights to flow conditions, such as velocity gradients, within the negative and positive skew surface features. OpenFOAM was chosen in part because it includes built-in functions to create unstructured meshes, which are preferred for complex geometries and accurate wall shear stress estimations, as well as second-order numerical schemes. Each attachment surface was modeled as a flat top surface moving at 0.83 m/s at a distance of 0.4 cm from a stationary flat bottom surface (the attachment surfaces), which matched the rotational speed and the gap between the inner and outer cylinders in the experiment. The dynamic viscosity of water was set to $8.9x10^{-4}$ Pa-s. The flat surface control was used for verification of OpenFOAM with the analytical solution.

For the skewed surfaces, a control volume mesh with dimensions of 900 μm (horizontal direction in Fig. 1a and b; X), 4000 μm (vertical direction; Y) and 100 μm (into the page; Z), was used to capture a representative section of each surface. The 3-dimensional mesh was effectively simplified to 2 dimensions to reduce computational times by modeling a single cell in the Z-direction, resulting in a control volume containing 7200 cells. Viscous forces were set to solve for a laminar steady state. A no-slip condition was specified at the solid–liquid interfaces. Periodic boundary conditions were set for the X-axis extents to remove any boundary effects: at the minimum and maximum extents of the X-axis (X ±), flow outputs from the X + boundary were inputs to the X- boundary. The one-cell Z ± boundaries were dictated by symmetry, and the Y ± boundaries were set by the solid surfaces and the no-slip condition. Initial conditions included a stationary fluid and a pressure of 0 Pa.

2.4. Statistics

Statistical significance was assessed using Student's *t*-test. T-tests and principal coordinate analyses (PCoAs, using Euclidean distances) were performed using Excel with the Real Statistics resource pack (Microsoft, Redmond, WA, USA). Nitrogen data was analyzed using multiple measurements from each of the experimental duplicate bioreactors over multiple days (i.e. days 19–23). Measurements were grouped from the replicate reactors, providing 6 to 10 measurements for each surface type where significant differences were calculated, except for day 34–49, when only 4 measurements from the negative skew reactor were included.

3. Results and discussion

3.1. Reactor performance

The effluent nitrite and nitrate concentrations from the 6 reactors (including experimental replicates for each surface type) were parsed into multi-day periods to facilitate data visualization and statistical analyses (Fig. 2). The average measured total effluent nitrogen for the flat, positive skewness, and negative skewness surfaces throughout the study was 29.8 ± 1.2, 29.6 ± 0.9, and 29.8 ± 0.8 mg-N/L respectively, which was 96–97% of the influent value of 30.8 mg-N/L, indicating reasonable nitrogen balances with minimal losses to processes such as

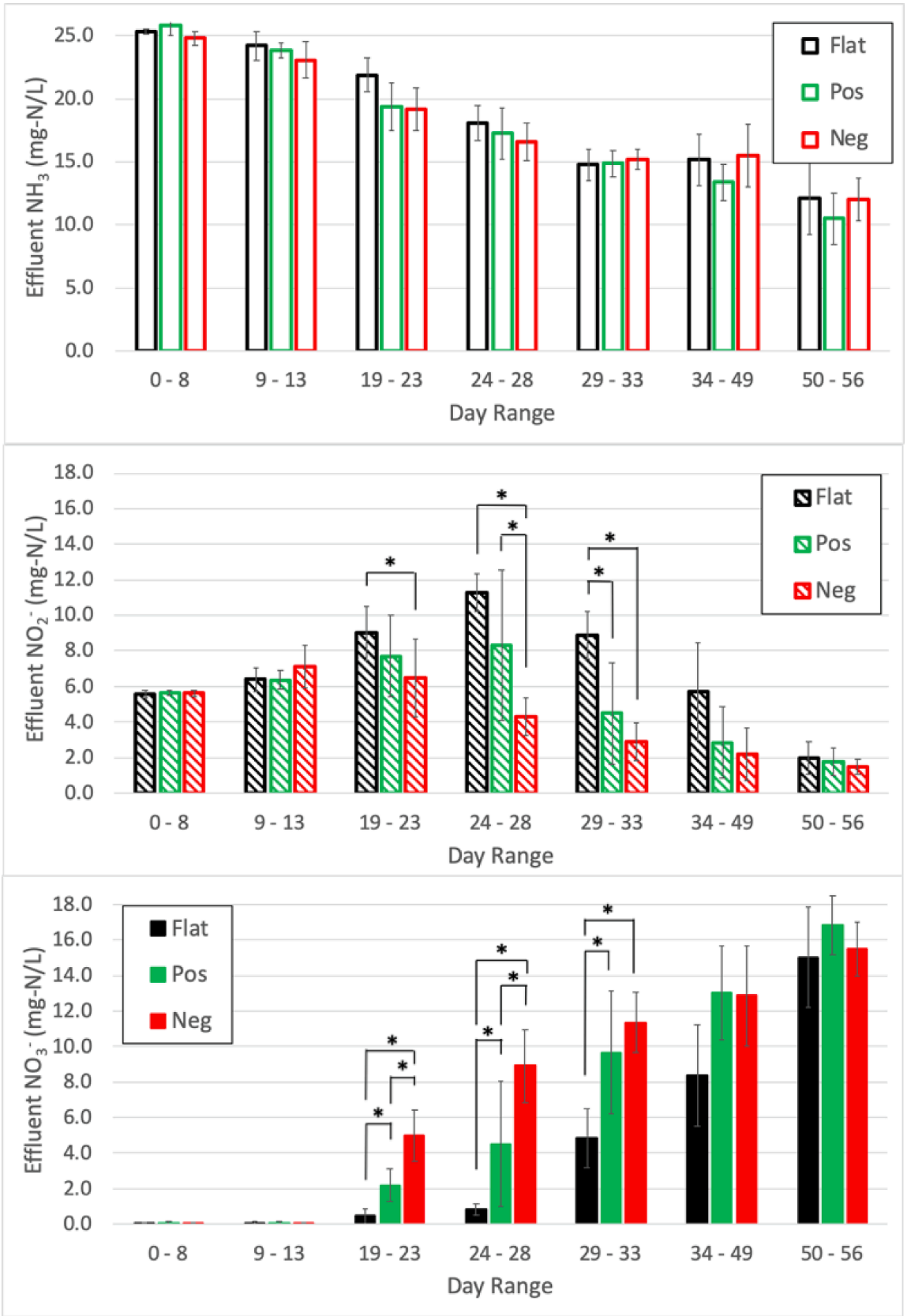

Fig. 2. (a) Effluent ammonia, (b) nitrite and (c) nitrate concentrations over the course of the experiment. Pos = positive skew surface, neg = negative skew surface. Influent ammonia, nitrite, and nitrate were 25, 5, and 0 mg N/L, respectively, and are shown with horizontal blue lines. Error bars show standard deviations of 6 to 10 measurements from replicate reactors sampled over multiple days, except for days 34–49, which includes 4 measurements from one negative skew reactor due to physical biofilm damage during sampling of the other reactor. Significant differences ($n \geq 6$, $p < 0.05$) are starred. (For interpretation of the references to colour in this figure legend, the reader is referred to the web version of this article.)

denitrification and assimilation.

Surface type had no measureable effect on the biofilms during the initial startup phase (through day 13; Fig. 2). There was no measurable activity at all through day 8, as indicated by effluent ammonia, nitrite, and nitrate concentrations near the influent values. During days 9–13, nitrite concentrations began to increase for all surfaces, with average nitrite production between 1.4 ± 0.5 and 2.1 ± 1.2 mg-N/L (Fig. 2b), while ammonia concentrations simultaneously decreased (Fig. 2a), indicating AOB activity had begun. Nitrate concentrations remained near zero days 9–13, however, indicating AOB activity preceded NOB activity even though nitrite was available in the nutrient feed (NOBs typically rely on AOB activity for nitrite production, but nitrite was supplied to avoid this limitation in this study).

By days 19–23, differences between the biofilm activities emerged, and were most apparent with regards to the onset of NOB activity (nitrate production). The negatively skewed surface produced the most rapid onset of NOB activity, followed by the positively skewed surface, and then the flat surface, with significantly different concentrations between all surfaces during days 19–23 ($p < 0.05$) (Fig. 2c). This trend continued throughout the middle phase of the study (days 19 to 33, Fig. 2c). During days 19–23 and 24–28 nitrate production was approximately twice that on the negatively skewed surface as on the positively skewed surface; for example, days 24–28 nitrate concentrations were 8.9 ± 2.1 mg-N/L and 4.5 ± 3.5 mg-N/L for the negative skewness and positive skewness surfaces, respectively. The onset of NOB activity was particularly slow in the flat surface reactors, with effluent nitrate concentrations remaining < 1 mg-N/L through day 28, suggesting a lag of at least 10 days for NOB activity on the flat surface relative to the skewed surfaces. By days 29–33, NOB activity on the negative skew surface (nitrate production 11.3 ± 1.7 mg-N/L) remained higher than the positive skew surface (nitrate production 9.7 ± 3.4 mg-N/L), but the difference between the measurements was no longer significant. After 44 days, biofilms on all surfaces had similar nitrite and nitrate concentrations, indicating that differences in nitrification rates had disappeared. The study was halted upon observation of similar performance between biofilms on all surfaces from days 50–56.

These results suggested that AOB activity rates were not greatly influenced by either skewness or surface roughness, as all surfaces yielded similar rates of ammonia uptake throughout the study (Fig. 2). In contrast, both roughness and skewness affected NOB growth, with the rougher surfaces (the positively and negatively skewed surfaces) exhibiting higher rates of NOB activity throughout the middle of the study than the flat surface, and the negatively skewed surface exhibiting higher rates of NOB activity than the positively skewed surface during this time. These differences were no longer evident by day 50, suggesting surface skewness and roughness primarily affected NOB activity before the biofilms had reached mature states. The finding that skewness apparently had a large effect on measured activity during biofilm development (approximately 33 days in this study) is noteworthy both because it suggests skew may be an important parameter for consideration during system startup, and also because most research on bacterial attachment to surfaces is performed over relatively short time frames, and so skewness effects should be considered in interpretation of results.

3.2. Biomass and microbial communities

Dry weight biomass measurements indicated that by day 26 the average biomass on the negative skew surface (0.7 mg/cm^2, n = 2) was higher than that on the positive skew (0.3 mg/cm^2, n = 2) and flat surfaces (0.4 mg/cm^2, n = 2) (Fig. 3). Biomass had increased on all surfaces by day 56, with the positive and negative skewness surface having similar average attached (average all 4 skew surfaces 0.78 ± 0.14 mg/cm^2), which was greater than that on the flat surface (0.50 and 0.51 mg/cm^2 in each of the flat surface reactors). The latter observation suggests the higher surface roughness of the skewed surfaces led to higher rates of biofilm attachment over the longer term, and was more important than differences in skewness. The finding that skewness apparently had a large effect over the short term, with over twice the attached biomass on the negative skew surfaces than the positive skew surfaces on day 26, supports the finding above that skewness affects biofilm development, which may be particularly important to improving system startup and research on bacterial attachment, as most attachment studies are performed over relatively short time frames.

The microbial communities on all surfaces were characterized by 16 s rRNA amplicon sequencing at the beginning (inoculant), middle (day 26) and end (day 53) of the experiment. It is important to note that the sequencing results provide information about relative abundances within each sample only, rather than absolute quantities, and that any rRNA PCR-based method can suffer from biases including variations in rRNA copy number, DNA extraction efficiencies, PCR amplification rates, and other errors (Lee et al., 2012). Population comparisons focused on the 30 genera that had an average relative abundance greater than 0.7% across all samples. This group accounted for 70–85% of all biofilm OTUs but comprised only 13.5% of the activated sludge inoculant OTUs, which was not surprising given the very different growth conditions (e.g., suspended versus biofilm) and feed between the

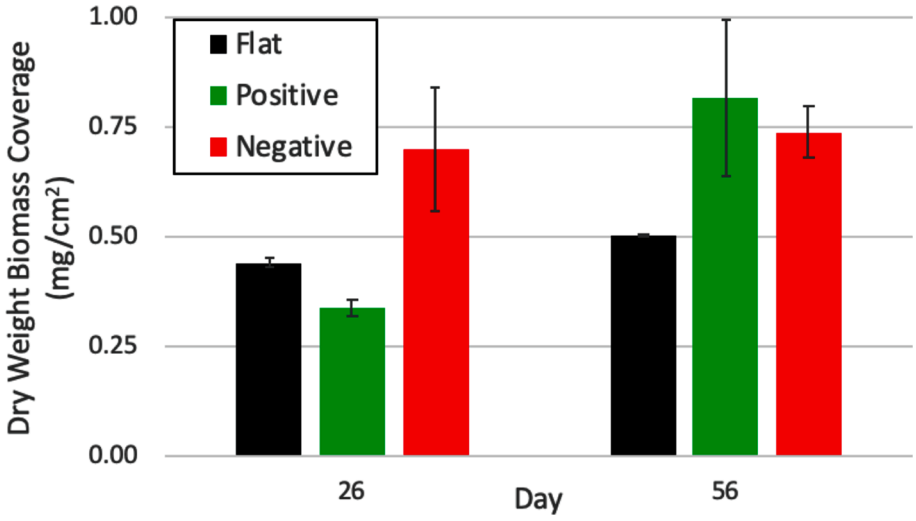

Fig. 3. Biomass on the flat, positive skewness, and negative skewness surfaces as dry weight per planer surface area (mg/cm^2). Error bars show ranges of experimental duplicate measurements.

wastewater plant and the laboratory reactors.

The most common detected genera are shown in Table 1. The inoculant contained a diverse bacterial population, with no genus comprising more than 5% of the total community (Table 1). On day 26, the bacterial communities across all biofilms were more similar to each other than they were to the activated sludge inoculant or to the day 53 samples, according to PCoA analysis (Fig. 4). This result suggested that variations in population composition on day 26 related to the differences in NOB activity (Fig. 2c) were small relative to overall population changes over the course of the experiment. By day 53 the flat surface biofilm community compositions had diverged considerably from the positive and negative skew surfaces, which remained similar in overall composition by PCoA analysis (Fig. 4).

Known autotrophic nitrifiers were identified in all samples. On day 26, the AOB *Nitrosomonas* was highest on the negative skew surface biofilms (average relative abundance 2%), followed by biofilms on the positive skewness surface (average 1.5%), and it was lowest on the flat surface (average 0.2%; Table 1), which was in agreement with the trend in ammonia uptake across these surfaces, although the differences in ammonia uptake were not statistically significant (Fig. 4). Known autotrophic NOB were detected across all biofilms on day 26 including *Nitrobacter* (ranging from 0.5 to 1.2%) and *Nitrospira* (ranging from 0.1 to 0.2%) (Table 1). The overall relatively low abundances of known autotrophic AOB and NOB are typical for previous studies, including systems fed excess ammonia (Liu et al. 2017).

The relative OTU abundances of known AOB and NOB were multiplied by the biomass quantities to obtain estimates of the mass abundances of various OTUs. While it is noted that biases such as DNA extraction amplification efficiencies can greatly affect results from PCR-based methods (Lee et al., 2012), this calculation is of interest because it accounts for differences both in biomass quantities (Fig. 3) and the OTU relative abundances (Table 1). Similar quantities of *Nitrobacter* on the flat, positive, and negative skew surfaces were calculated (3.5, 4.2, and 3.5 μg/cm^2, respectively), suggesting that differences *Nitrobacter* populations did not explain the overall differences in observed nitrate production (Fig. 2). The calculated quantities of *Nitrospira* on the flat, positive, and negative skew surfaces were 0.4, 0.2, and 1.2 μg/cm2 respectively. The relatively high *Nitrospira* abundance on the negative skew surface was consistent with the higher nitrate production on the negative skew surface (8.9 mg N/L), but *Nitrospira* quantities did not explain the greater nitrate production on the positive skew surface (4.5 mg N/L) than the flat surface (<1 mg N/L).

Differences in the activities of microbial populations on the different surfaces (e.g., more active NOB populations on the positive skew surface than on the flat surface) could help to explain these differences. For example, the day 26 nitrate production on the flat surface remained <1 mg N/L, but *Nitrobacter* and *Nitrospira* quantities were comparable to the positive and negative skew surfaces, suggesting that while present, these NOBs were apparently less active than on the other surfaces. Location in the biofilm, for example, would affect activity, with populations nearer the biofilm surface more active due to lower resistance to mass transport. Differences in the hydrodynamic (mixing) conditions in the liquid phase near the biofilm surfaces: as described in the hydrodynamic modeling discussion below, the negative skew surface had higher shear velocities across the largest surface area, followed by the positive skew surface and then the flat surface, which was consistent with the order of nitrate production on days 19–33. Another possible factor affecting the N transformation rates is the potential activity of heterotrophic nitrifiers, which are as described in more detail below.

Autotrophic nitrifiers became more prevalent from days by day 53, which was consistent with increases in nitrification rates during this time (Fig. 2). *Nitrosomonas* abundance increased to 3.2–5.2% and *Nitrospira* increased to a range of 0.7 – 7.8%, although only a single community had a relative abundance above 2.5% (Table 1). *Nitrobacter* relative abundance remained low and was similar to day 26 (0.5–0.6%).

Heterotrophic genera were the major drivers for the community differences revealed by the Euclidean distance-based PCoA analysis (Fig. 4), as autotrophic nitrifier communities represented relatively low fractions of the populations across all biofilms. On day 26 the most common genera were the heterotrophs *Acinetobacter* (16.9–23.3%), *Acidovorax* (12.3–16.9%), and *Hyphomicrobium* (6.0–14.0%) (Table 1). *Acinetobacter* species have been reported as early biofilm colonizers (Balasubramanian et al. 2012), including in a nitrification system (Lu et al. 2016), and they have also been identified as bridging organisms in floc formation (Malik et al., 2003). It is therefore possible this genus was important to early formation of biofilm structure in the current study, a hypothesis supported by the later decrease of *Acinetobacter* by more than an order of magnitude by day 53 (to 0.6–1.2% across all surfaces). Additionally, an *Acinetobacter* species isolated from activated sludge was found to oxidize ammonia and nitrite under aerobic conditions (Ren

Table 1
Genus with the highest average relative abundances (%) throughout the study, shown as heat map with low = red, high = green, and ordered from most common to least common for Day 26 values. Days 26 and 53 show average values from experimental replicate surfaces.

	DAY 0	DAY 26			DAY 53		
Genus	Inoculant	Flat	Positive	Negative	Flat	Positive	Negative
Acinetobacter	0.4	17.1	16.9	23.3	0.6	1.0	1.2
Acidovorax	0.6	16.9	12.3	14.7	11.0	17.1	16.0
Hyphomicrobium	0.8	9.2	14.0	6.0	7.2	2.9	3.2
Terrimonas	0.6	1.4	1.1	8.6	7.4	2.0	6.6
Comamonas	1.2	5.6	2.9	2.5	1.3	1.6	1.5
Acidobacterium	1.5	8.0	2.3	0.8	1.3	0.6	0.3
Brevundimonas	0.0	2.2	3.5	3.8	1.0	0.6	0.7
Rhodobacter	0.9	1.8	3.7	3.4	2.3	1.1	1.0
Sphingopyxis	0.1	2.6	2.5	2.9	7.0	2.3	2.1
Shinella	0.0	1.6	2.4	1.4	1.2	0.5	0.4
Flavihumibacter	0.1	0.7	3.8	1.1	8.1	1.1	1.9
Nitrosomonas	0.5	0.2	1.5	2.0	3.2	5.2	4.9
Nitrobacter	0.1	0.8	1.2	0.5	0.5	0.5	0.6
Nitrospira	1.2	0.1	0.1	0.2	1.4	0.7	7.8
Unknown OTU	0.1	0.0	0.0	0.0	1.3	11.8	10.6

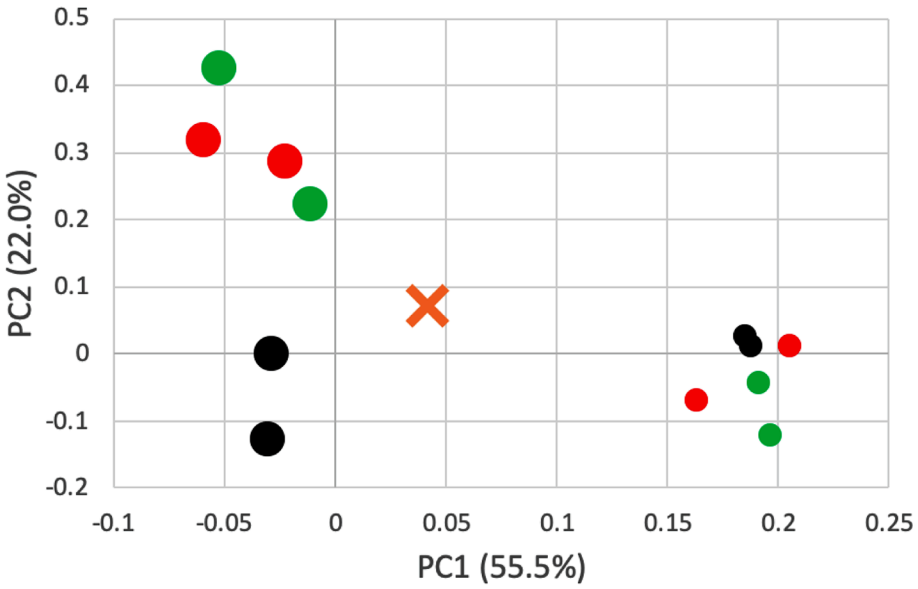

Fig. 4. PCoA of microbial communities identified at genus level, as determined by 16 s rRNA amplicon sequences. Activated sludge inoculant = orange X, flat surface biofilms = black, positive skewness = green, negative skewness = red. (For interpretation of the references to colour in this figure legend, the reader is referred to the web version of this article.)

et al., 2014), suggesting it could play a role in nitrogen transformations in some systems.

The high fractions of *Acidovorax* across all biofilms on days 26 and 53 were particularly interesting, as this genus has been suggested to perform heterotrophic nitrification within activated sludge processes (Fu and Zhao, 2015), and application of stable isotope probing (SIP) recently indicated it took up radiolabelled bicarbonate under conditions favoring ammonia oxidation, which suggested this genus may include autotrophic AOBs (Gülay et al., 2019). Further research is needed to determine whether species within this genus actually do act as AOBs, but its high relative abundances in this study, with no added organic carbon and measured ammonia oxidation, support this hypothesis. *Acidovorax* fractions were higher on the positive skew (average 17.1%) and negative skew surfaces (16%) than the flat surface (11.0%) on day 53, which contributed to the differences between the day 53 skewed and flat surfaces in the PCoA analysis (Fig. 4).

One of the larger differences between the biofilms on day 26 was the much higher fraction of *Terrimonas* in the negative skew biofilm (average 8.6%) than the flat and positive skew biofilms (averages 1.4 and 1.1%, respectively). *Terrimonas'* role in the current study is not known but these differences may be notable because on day 26 the negative skewness surface biofilms exhibited much higher NOB activity than the other biofilms (Fig. 2c). *Terrimonas* has been frequently found in simultaneous nitrification/denitrification systems, and although it has been suggested to be an aerobic denitrifier (Liu et al., 2020), its magnified presence in the biofilms with the highest NOB activity raise the question of whether it could act as an NOB. Further research is needed to determine its precise role.

On Day 53 an unidentified OTU appeared at relatively high fractions in the positive and negative skew surface biofilms (11.2 ± 6.2%, n = 4), while this OTU was scarce in the flat surface biofilms (Table 1). The uncultured OTU was found to co-vary closely with *Nitrosomonas* using hierarchical cluster analysis (data not shown). While this result may suggest that the unidentified bacterium could have nitrifying capabilities or could be linked with AOB proliferation, but further research is needed on this point.

3.3. Computational fluid dynamics analyses and scanning electron microscopy

CFD modeling was used to gain a better understanding of how the different topographies may have affected biofilm attachment and growth. As described above, flow conditions were simulated in a simplified system consisting of 2 flat parallel plates using OpenFOAM modelling software. The focus of these analyses was on local shear stresses, as these provide an indication of velocity gradients, which in turn drive mass transport (both for transport of cells to the surfaces during initial adhesion and transport of metabolites to and from attached biofilms).

The CFD simulations predicted the same uniform shear stress on the moving flat surface (0.18 Pa) as did the analytical solution for concentric cylinders (Eq.2), which provided some confirmation of the CFD model. The predicted shear stress along the positive skewness surface varied from negligible values along the trough sections to 8.5 Pa at the upstream peak (Fig. 5a and c), while the maximum shear stresses along the negative skew surface were 4.1 Pa (Fig. 5b and d). The shear stress values along each surface are shown in Fig. 5c and d, which illustrate that while the positive skew surfaces had higher maximum values than the negative skew surface, more of the negative skew surface was exposed to relatively high shear forces. For example, 19% of the positive skew surface had shear stress values greater than 1 Pa, while 59% of the negative skew surface had shear stress values greater than 1 Pa (shaded regions in Fig. 5c and d, respectively). Higher velocity gradients tend to increase mass transport rates of nutrients and electron acceptors, for example, by increasing advective flow to biofilm surfaces and by decreasing the laminar boundary layer thickness, which is in turn favorable to biofilm growth and activity (Tsagkari and Sloan, 2018). It is therefore hypothesized that the predicted greater area with high shear values on the negative skew surface relative to the positive skew surface (Fig. 5c and d) was indicative of increased mass transport to the surface, which would explain the greater rates of biofilm attachment, growth, and activity through day 33 on the negative skew surface relative to the other surfaces (Fig. 2). This hypothesis is supported by previous studies that show increased wall shear stress has been associated with higher bacterial adhesion (Saur et al., 2017). Rochex et al. (2008) also reported that shear stress influenced the composition and diversity of biofilm microbial communities. The CFD results therefore provide a possible

explanation for the higher rates of biofilm development and activity found on the negative skewness surfaces than the positive skewness and flat surfaces through day 33. After this time, the biofilms grown on the 3 surfaces were more similar (Fig. 2, days 50–56), and it was hypothesized that this may have been due to overgrowth of the surface features by the biofilms.

SEM imaging of biofilm growth generally supported the above hypotheses. On day 26, biomass on the surface with positive skewness surface appeared to be evenly and lightly distributed across the surface, with the silicone surface clearly visible. In contrast, the biomass on the negative skewness surface was concentrated along the rounded-peaks, obscuring the attachment surface and appearing more dense than the biofilm on the positive skewness surface. The troughs were clearly visible, indicating little or no growth, corresponding to the areas with the predicted lowest shear values. These observations were consistent with the hypothesis suggested above that the higher shear stress along the rounded peaks of the negative skewness surfaces were preferred attachment sites and/or they provided zones of increased mass transfer to accelerate biofilm growth. In contrast, the high shear zones predicted on the positive skew surface (near the sharp peaks, Fig. 5a and c) were not obviously associated with increased attached biomass. It is possible that the very high shear rates over a small area near the positive skew peaks (the maximum shear of 8.5 Pa was over twice the maximum shear of 4.1 Pa on the negative shear surface) negatively affected biomass adhesion and biofilm development because of the shear forces, which may have overwhelmed any benefits associated with increased mass transfer rates.

By day 53, the surfaces with positive and negative skewness both exhibited more uniform biofilm coverage, which had begun to obscure the underlying peaks and troughs, which was consistent with their similar dry weight measurements on day 56 (Fig. 3). The skewness surface types each had higher biomass coverage (0.8 and 0.7 mg/cm^2 for the positive and negative skewness surfaces, respectively) than the flat surface (0.5 mg/cm^2), which may have been due to their greater roughness than the flat surface. It is notable that these differences in attached biomass did not greatly affect the rates of nitrogen transformations (Fig. 2), suggesting the flat surface biofilm was more active per unit mass than the other surfaces. The reasons for these result are not known, but the similar rates of nitrogen transformations across all surfaces at the end of the experiment indicates similar flux values (activity per surface area) across all surfaces, which in turn suggests that biofilm activities were limited by the biofilm surface areas, as could occur if biofilm activity were concentrated in the biofilm closest to the bulk fluid, which is consistent with expectations based on mass transfer limitations and proximity to ammonia, oxygen, and other substrates.

3.4. Relevance to biological surfaces

These results may be particularly relevant to the study of biological surfaces. The skin surfaces of many aquatic organisms have been extensively studied to determine the functions of various features, often with the goal of developing biomimetic engineering design strategies. For example, shark skin is composed of ridges (riblets) spaced at approximately 50 μm arranged on tooth-like structures called denticles. The functions of these structures have been the subject of much fluid dynamics and biological research over the last 35 years. While it has often been suggested that the riblets serve to reduce drag, more recent research has indicated that the overall structures may actually increase

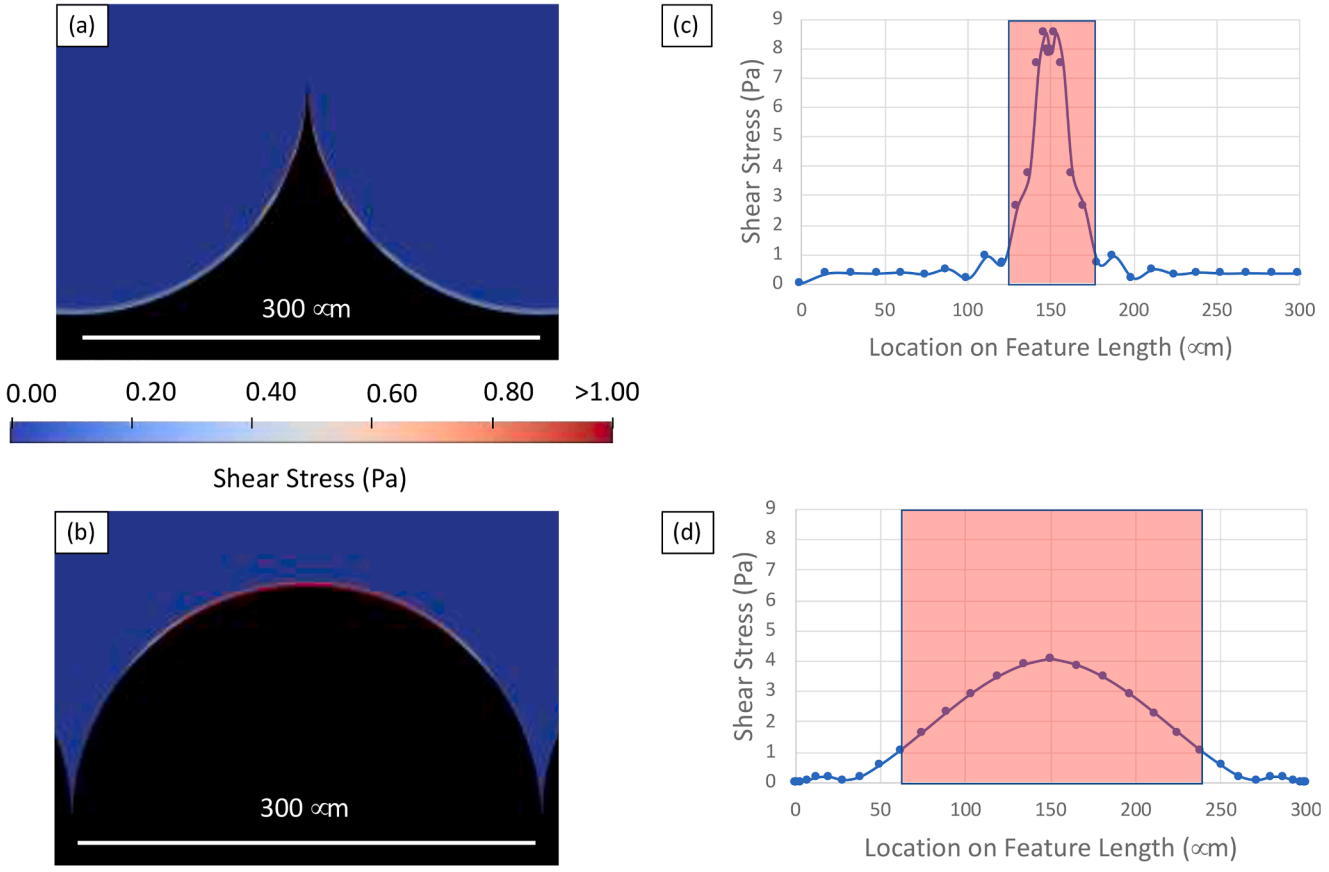

Fig. 5. CFD model results. Simulated shear stress profiles along surfaces with (a) positive and (b) negative skewness along representative feature lengths. Fig.s (c) and (d) show shear stress values at the surface/water interface for the positive and negative skewness surfaces, respectively, for the data shown in (a) and (b). Pink shaded sections indicate shear values greater than 1 Pa. (For interpretation of the references to colour in this figure legend, the reader is referred to the web version of this article.)

drag (Boomsma and Sotiropoulos, 2016). These surfaces possess a pronounced positive skew, with the riblet points providing sharp peaks similar to Fig. 1a, and so the research presented herein suggests these features could also serve to reduce microbial attachment. Multiple studies have evaluated turbulence structures associated with these surface features, and have suggested that riblets tend to isolate high shear stresses near the tips while providing low stress regions in the valleys between tips (Boomsma and Sotiropoulos, 2016; Choi et al. 1993), which is consistent with the CFD results shown in Fig. 5. Further research is needed to determine the potential benefits of positive skew on biological surfaces to reduce drag and/or microbial attachment, which could be important in the selection or biomimetic design of skew on synthetic surfaces for application in systems where control of drag and/or biofilms is desirable. These findings may be useful to consider both in systems where biofilm development is desired, such as in wastewater treatment, and for design of other systems where reduced attachment is desired, such as pipelines. Additional research is needed to determine the importance of skewness on biofilms relative to other parameters such as surface chemistry, roughness, kurtosis, and periodicity.

4. Conclusions

This article describes the first study of bacteria adhesion and development on surfaces specifically engineered to possess opposite skewness and identical roughness values, thereby enabling the controlled study of skewness effects. The results suggest that surface skewness can affect biofilm development and activity in thin biofilms, where surface features are not overgrown, including shorter-term studies common in the bacterial attachment and development literature, and also many natural and industrial systems. Application of these results to improving engineered systems could include considering variations in skewness that occur with different materials (Lüdecke et al., 2014) and manufacturing or finishing processes.

CRediT authorship contribution statement

Philip M. Roveto: Methodology, Investigation, Formal analysis, Writing - original draft. **Adwaith Gupta:** Software. **Andrew J. Schuler:** Conceptualization, Resources, Writing - review & editing, Supervision.

Declaration of Competing Interest

The authors declare that they have no known competing financial interests or personal relationships that could have appeared to influence the work reported in this paper.

Acknowledgements

This work was supported by National Science Foundation, Grant 1345169. Special thanks to Curtis Hunt and Dennis Martinez for data acquisition.

Appendix A. Supplementary data

Supplementary data to this article can be found online at https://doi.org/10.1016/j.biortech.2020.124251.

References

American Public Health Association, American Water Works Association and Water Environment Federation (2005). Standard Methods for the Examination of Water and Wastewater. Washington, D.C.

Andereck, C.D., Liu, S.S., Swinney, H.L., 1986. Flow regimes in a circular Couette system with independently rotating cylinders. J. Fluid Mech. 164, 155–183.

Balasubramanian, V., Palanichamy, S., Subramanian, G., Rajaram, R., 2012. Development of polyvinyl chloride biofilms for succession of selected marine bacterial populations. J. Environ. Biol. 33 (1), 57–60.

Balows, A., Trüper, H.G., Dworkin, M., Harder, W., Schleifer, K.-H. (Eds.), 1992. The Prokaryotes. Springer New York, New York, NY https://doi.org/10.1007/978-1-4757-2191-1.

Boomsma, A., Sotiropoulos, F., 2016. Direct numerical simulation of sharkskin denticles in turbulent channel flow. Phys. Fluids 28, 035106.

Choi, H., Moin, P., Kim, J., 1993. Direct numerical simulation of turbulent flow over riblets. J. Fluid Mech. 255 (-1), 503. https://doi.org/10.1017/S0022112093002575.

Chung, K.K., Schumacher, J.F., Sampson, E.M., Burne, R.A., Antonelli, P.J., Brennan, A. B., 2007. Impact of engineered surface microtopography on biofilm formation of *Staphylococcus aureus*. Biointerphases 2 (2), 89–94.

Crawford, R.J., Webb, H.K., Truong, V.K., Hasan, J., Ivanova, E.P., 2012. Surface topographical factors influencing bacterial attachment. Adv. Colloid Interface Sci. 179-182, 142–149.

DeSantis, T.Z., Hugenholtz, P., Larsen, N., Rojas, M., Brodie, E.L., Keller, K., Huber, T., Dalevi, D., Hu, P., Andersen, G.L., 2006. Greengenes, a Chimera-Checked 16S rRNA Gene Database and Workbench Compatible with ARB. AEM 72 (7), 5069–5072.

Fu, Z., Zhao, J., 2015. Impact of quinoline on activity and microbial culture of partial nitrification process. Bioresour. Technol. 197, 113–119.

Gülay, A., Fowler, S.J., Tatari, K., Thamdrup, B., Albrechtsen, H.-J., Al-Soud, W.A., Sørensen, S.J., Smets, B.F., 2019. DNA- and RNA-SIP Reveal *Nitrospira* spp. as Key Drivers of Nitrification in Groundwater-Fed Biofilters. mBio 10 (6), e01870–19. https://doi.org/10.1128/mBio.01870-19.

Hall-Stoodley, L., Costerton, J.W., Stoodley, P., 2004. Bacterial biofilms: from the Natural environment to infectious diseases. Nat. Rev. Microbiol. 2 (2), 95–108.

Khan, M.M.T., Chapman, T., Cochran, K., Schuler, A.J., 2013. Attachment surface energy effects on nitrification and estrogen removal rates by biofilms for improved wastewater treatment. Water Res. 47 (7), 2190–2198.

Khan, M.M.T., Ista, L.K., Lopez, G.P., Schuler, A.J., 2011. Experimental and theoretical examination of surface energy and adhesion of nitrifying and heterotrophic bacteria using self-assembled monolayers. Environ. Sci. Technol. 45 (3), 1055–1060.

Kim, Y.H., Cho, J.H., Lee, Y.W., Lee, W.K., 1997. Development of a carrier for adhesion of nitrifying bacteria using a thermodynamic approach. Biotechnol. Tech. 11, 773–776. https://doi.org/10.1023/A:1018460805328.

Klaus, S., McLee, P., Schuler, A.J., Bott, C., 2016. Methods for increasing the rate of anammox attachment in a sidestream deammonification MBBR. Water Sci. Technol. 74 (1), 110–117.

Lee, C.K., Herbold, C.W., Polson, S.W., Wommack, K.E., Williamson, S.J., McDonald, I.R., Cary, S.C., 2012. Groundtruthing next-gen sequencing for microbial ecology-biases and errors in community structure estimates from PCR amplicon pyrosequencing. PLoS ONE 7 (9), e44224.

Liu, T., Mao, Y.-jun., Shi, Y., Quan, X., 2017. Start-up and bacterial community compositions of partial nitrification in moving bed biofilm reactor. Appl. Microbiol. Biotechnol. 101 (6), 2563–2574.

Liu, T., He, X., Jia, G., Xu, J., Quan, X., You, S., 2020. Simultaneous nitrification and denitrification process using novel surface-modified suspended carriers for the treatment of real domestic wastewater. Chemosphere 247, 125831.

Lu, H., Xue, Z., Saikaly, P., Nunes, S.P., Bluver, T.R., Liu, W.-T., 2016. Membrane biofouling in a wastewater nitrification reactor: Microbial succession from autotrophic colonization to heterotrophic domination. Water Res. 88, 337–345.

Lüdecke, C., Jandt, K.D., Siegismund, D., Kujau, M.J., Zang, E., Rettenmayr, M., Bossert, J., Roth, M., 2014. Reproducible biofilm cultivation of chemostat-grown Escherichia coli and investigation of bacterial adhesion on biomaterials using a non-constant-depth film fermenter. PLoS ONE 9 (1), e84837. https://doi.org/10.1371/journal.pone.0084837.

Malik, A., Sakamoto, M., Hanazaki, S., Osawa, M., Suzuki, T., Tochigi, M., Kakii, K., 2003. Coaggregation among nonflocculating bacteria isolated from activated sludge. AEM 69 (10), 6056–6063.

Martens-Habbena, W., Berube, P.M., Urakawa, H., de la Torre, José.R., Stahl, D.A., 2009. Ammonia oxidation kinetics determine niche separation of nitrifying Archaea and Bacteria. Nature 461 (7266), 976–979.

Nowka, B., Daims, H., Spieck, E., 2015. Comparison of Oxidation Kinetics of Nitrite-Oxidizing Bacteria: Nitrite Availability as a Key Factor in Niche Differentiation. Appl. Env. Microbiol. 81, 745–753. https://doi.org/10.1128/AEM.02734-14.

Ren, Y.-X., Yang, L., Liang, X., 2014. The characteristics of a novel heterotrophic nitrifying and aerobic denitrifying bacterium, *Acinetobacter junii YB*. Bioresour. Technol. 171, 1–9.

Rochex, A., Godon, J., Bernet, N., Escudie, R., 2008. Role of shear stress on composition, diversity and dynamics of biofilm bacterial communities. Water Res. 42 (20), 4915–4922.

Roveto, P.M., Schuler, A.J., 2019. Performance and diversity responses of nitrifying biofilms developed on varied materials and topographies to stepwise increases of aeration. Bioresour. Technol. 281, 429–439.

Santoro, C., Artyushkova, K., Babanova, S., Atanassov, P., Ieropoulos, I., Grattieri, M., Cristiani, P., Trasatti, S., Li, B., Schuler, A.J., 2014. Parameters characterization and optimization of activated carbon (AC) cathodes for microbial fuel cell application. Bioresour. Technol. 163, 54–63.

Saur, T., Morin, E., Habouzit, F., Bernet, N., Escudié, R., 2017. Impact of wall shear stress on initial bacterial adhesion in rotating annular reactor. PloS ONE 12 (2).

Sedlaček, M., Podgornik, B., Vižintin, J., 2012. Planning surface texturing for reduced friction in lubricated sliding using surface roughness parameters skewness and kurtosis. Proc. Inst. Mech. Eng. Part J: J. Eng. Tribol. 226 (8), 661–667.

Singh, A.V., Vyas, V., Patil, R., Sharma, V., Scopelliti, P.E., Bongiorno, G., Podestà, A., Lenardi, C., Gade, W.N., Milani, P., 2011. Quantitative characterization of the influence of the nanoscale morphology of nanostructured surfaces on bacterial adhesion and biofilm formation. PLoS ONE 6 (9). https://doi.org/10.1371/journal.pone.0025029.

Song, Z., Zhang, X., Ngo, H.H., Guo, W., Song, P., Zhang, Y., Wen, H., Guo, J., 2019. Zeolite powder based polyurethane sponges as biocarriers in moving bed biofilm reactor for improving nitrogen removal of municipal wastewater. Sci. Total Environ. 651, 1078–1086.

Tayebi, N., Polycarpou, A.A., 2004. Modeling the effect of skewness and kurtosis on the static friction coefficient of rough surfaces. Tribol. Int. 37 (6), 491–505.

Tsagkari, E., Sloan, W.T., 2018. Turbulence accelerates the growth of drinking water biofilms. Bioprocess Biosyst. Eng. 41 (6), 757–770.

Turner, S., Pryer, K.M., Miao, V.P., Palmer, J.D., 1999. Investigating deep phylogenetic relationships among cyanobacteria and plastids by small subunit rRNA sequence analysis. J. Eukaryot. Microbiol. 46, 327–338. https://doi.org/10.1111/j.1550-7408.1999.tb04612.x.

van den Akker, B., Holmes, M., Pearce, P., Cromar, N.J., Fallowfield, H.J., 2011. Structure of nitrifying biofilms in a high-rate trickling filter designed for potable water pre-treatment. Water Res. 45 (11), 3489–3498.

Weller, H.G., Tabor, G., Jasak, H., Fureby, C., 1998. A tensorial approach to computational continuum mechanics using object-oriented techniques. Comput. Phys. 12 (6), 620–631. https://doi.org/10.1063/1.168744.

Whitehead, K.A., Verran, J., 2006. The effect of surface topography on the retention of microorganisms. Food Bioprod. Process. 84 (4), 253–259.